Predictability of the Indian monsoon in coupled general circulation models

V. Krishnamurthy and J. Shukla

Center for Ocean-Land-Atmosphere Studies
Institute of Global Environment and Society
Calverton, Maryland, USA
and
Department of Atmospheric, Oceanic and Earth Sciences
George Mason University
Fairfax, Virginia, USA

Chapter 7

Monsoon Monographs, Volume II, 2012, (pages 266-306)

Editors: Ajit Tyagi et. al.

Abstract

The predictability of the Indian monsoon rainfall and circulation in eight coupled ocean-atmosphere models is reviewed. The retrospective forecasts generated by the Climate Forecast System (CFS) of the U.S. National Centers for Environmental Prediction and by seven European coupled models from the Development of a European Multimodel Ensemble System for Seasonal-to-Interannual Prediction (DEMETER) project are analyzed. The predictability of these eight models at daily and seasonal time scales is discussed in terms of forecast errors which include the imperfections in both the model and initial condition and predictability errors which depend solely on the uncertainties in the initial condition assuming the model to be perfect. The doubling time of small errors was estimated to be about 4-14 days in the CFS and about 4-7 days in the DEMETER models for the rainfall over India. No model was successful in capturing the observed interannual variability of the seasonal mean monsoon rainfall whereas all the models were able to better forecast the surface temperature of the equatorial Pacific. Large errors in the seasonal anomalies of the rainfall occur in the Bay of Bengal, the Arabian Sea along the west coast of the Indian Peninsula and the equatorial Indian Ocean. The relation between the Indian monsoon and the decadal oscillations of different ocean basins are also discussed.

1. Introduction

Because of the tremendous impact of monsoon on various socio-economic aspects of India, the prediction of the monsoon rainfall was recognized to be crucial more than a hundred years ago. The India Meteorological Department (IMD) has long been issuing seasonal forecasts of rainfall using statistical prediction schemes that took firm root with the discovery of significant correlation between the seasonal rainfall and various regional and global climate phenomena by Walker (1923, 1924). Some of these predictors are based on now well-known slowly-varying components of the climate systems such as El Niño-Southern Oscillation (ENSO) (Krishnamurthy and Kinter 2003). Many developing El Niño (La Niña) events have coincided with below-normal (above-normal) seasonal monsoon rainfall (Sikka 1980; Rasmusson and Carpenter 1983). The dynamical basis for long-range prediction of seasonal mean monsoon rainfall was established by general circulation model (GCM) experiments which showed that the tropical atmospheric variability is largely determined by slowly-varying boundary forcings such as sea surface temperature (SST), soil moisture and snow cover (Charney and Shukla 1981).

The Charney-Shukla hypothesis was further supported by observational evidence and was modified by Krishnamurthy and Shukla (2000, 2007, 2008) who suggested that the interannual variability of the seasonal mean monsoon consists of large-scale seasonally persistent component and a statistical average of intraseasonal variations. They found two nonlinear oscillations, a northeastward propagating mode with an average period of 45 days and a northwestward propagating mode with a period of 30 days, which largely explained the active and break phases

of the monsoon. The seasonal mean monsoon, however, was accounted for by two seasonally persisting modes that were shown to be related to ENSO and Indian Ocean Dipole (IOD). The seasonal mean monsoon is determined by the relative strengths of these persistent ENSO and IOD atmospheric modes which can interfere either constructively or destructively. For example, the seasonal rainfall in 1997, the strongest El Niño year on record, was normal because of the counteracting effect of the atmospheric ENSO and IOD modes. The persistent atmospheric modes were shown to have strong lead/lag correlation with the SSTs of the Indian and Pacific oceans (Krishnamurthy and Kirtman 2009), indicating the strong predictive potential of the SST.

The statistical forecasting method employed by the IMD has met with varying degree of success but with no improvement in the forecast skill over a long period (Rajeevan 2001; Gadgil et al. 2005). This method has limitations because it does not provide forecasts with spatial distribution of the rainfall or on sub-seasonal time scales. There are more fundamental problems related to the use of limited amount of data and the choice of the predictors (Lorenz 1962, DelSole and Shukla 2002). On the other hand, the dynamical prediction has evolved over the years to a stage where coupled GCMs are now employed for routine seasonal climate prediction by operational forecasting centers. Earlier studies of dynamical prediction of the Indian monsoon relied on atmospheric GCMs using observed SST as boundary forcing (Palmer et al. 1992; Sperber and Palmer 1996; Krishnamurthy and Shukla 2001; Sperber et al. 2001; Kang et al. 2002). Most of these models simulated the monsoon with deficit rainfall over northern India and excess rainfall over the Arabian Sea and the Bay of Bengal. The interannual variability of the seasonal rainfall in the models showed poor correlation with observations although SST seems to have strong influence. Although this two-tier approach has served useful purpose, Wang et al. (2005) showed that the observed lagged correlation between SST and rainfall was correctly

simulated by a coupled GCM but not by an atmospheric GCM forced with observed SST, especially in the subtropical western Pacific where SSTs are primarily forced by the atmosphere. These results emphasize the importance of the coupled ocean-atmosphere interaction in the monsoon region and the need to use coupled GCMs for better prediction. The prediction skill of the monsoon was found to be better with a coupled model compared to that using an atmospheric model (Kumar et al. 2005).

The objective of this review is to discuss the predictability of coupled GCMs in simulating the Indian monsoon. According to Lorenz (1984), the predictability of a system is the degree of accuracy with which it is possible to predict the state of the system in the future. It is worth emphasizing that predictability always refers to the specific model that is used to make the prediction. The relevance of the specific phenomenon, such as monsoon, that is predicted may appear through the time scales and the instabilities involved. The models assessed in this study are advanced coupled GCMs that are used either for operational forecasts of seasonal climate or for developing new approaches to seasonal prediction. The model that is discussed in more detail is the Climate Forecast System (CFS) version 1 of the U.S. National Centers for Environmental Prediction (NCEP). The CFS has been providing operational seasonal predictions since 2004 (Saha et al. 2006). The other models, developed at seven European institutions, come from a project called the Development of a European Multimodel Ensemble System for Seasonal-to-Interannual Prediction (DEMETER) (Palmer et al. 2004). Retrospective forecasts generated by these models have been analyzed to assess their predictability.

The predictability of weather models is usually assessed by analyzing the growth of daily errors and finding the growth rate and doubling time of errors. The daily weather forecasts of the European Centre for Medium Range Forecasts (ECMWF) were examined by Lorenz (1982) who

estimated the doubling time of small errors in the midlatitudes to be about 2-2.5 days. Similar estimates were obtained in the subsequent assessments of the ECMWF weather forecasts (Simmons and Hollingsworth 2002). The Lorenz method was used in recent studies (Rai and Krishnamurthy 2011, Krishnamurthy and Rai 2011) to assess the predictability of the Indian monsoon rainfall and circulation in NCEP CFS. The doubling time of errors was estimated to be about 4-5 days for forecasts initiated during the peak monsoon period. Since these errors saturate in a matter of few days, the analysis of errors in instantaneous states is not suitable for predictability on climate time scales (e.g., seasonal forecasts). For the tropics, Shukla (1998) has shown that the differences between simulations with the same SST forcing are much less than the differences between simulations with different SST forcings, emphasizing the role of slower components in climate predictability. In an analysis of the seasonal forecasts of the monsoon, the CFS was found to predict the ENSO-related features of the monsoon better than the regional features that may not be strongly influenced by SST (Drbohlav and Krishnamurthy 2010).

The predictability of the DEMETER coupled models was compared with the predictability of observed SST forced atmospheric GCMs of the Asia-Pacific Economic Cooperation Climate Network by Kang and Shukla (2006). The atmospheric models produced large systematic errors in the monsoon region, and the predictions showed poor correlation skill. There was no improvement in the correlation skill with the multimodel composite approach. However, the DEMETER coupled models showed better predictability of the seasonal mean rainfall over the monsoon region and western Pacific, indicating the importance of ocean-atmosphere interaction. The multimodel composites of the DEMETER model predictions of the summer season rainfall also had better spatial correlation skill.

In section 2, the CFS and the DEMETER models are described along with details of the

retrospective forecasts generated by these models. The predictability of the daily rainfall and circulation is discussed in section 3. Section 4 discusses the seasonal mean monsoon and its predictability. A discussion of the potential for the predictability of monsoon on decadal time scale is provided in section 5. A summary is given in section 6.

2. Models and retrospective forecasts

a. NCEP Climate Forecast System

The NCEP CFS consists of Global Forecast System (GFS) as its atmospheric component (Moorthi et al. 2001) while the Geophysical Fluid Dynamics Laboratory (GFDL) Modular Ocean Model version 3 (MOM3) is its oceanic component (Pacanowski and Griffies 1998). The GFS has T62 horizontal resolution along with 64 sigma vertical layers. The MOM3 has a zonal resolution of 1°, meridional resolutions of 1/3° in the extratropics and 1° in the tropics and 40 layers in the vertical. The atmospheric and oceanic models exchange momentum and heat fluxes once a day with no flux correction. The ocean model is prescribed with observed climatology of the sea ice extent. The initial conditions for the atmospheric model is obtained from the NCEP-Department of Energy Atmospheric Model Intercomparison Project (AMIP II) Reanalysis-2 (R2; Kanamitsu et al. 2002) while the NCEP Global Ocean Data Assimilation System provides the initial conditions for the ocean model. More details of the CFS are given by Saha et al. (2006).

The retrospective forecasts were generated at NCEP by integrating the CFS starting each month for the period 1981-2005. Each ensemble of nine-month long retrospective forecasts consists of 15 members starting from different initial conditions each month. For example, the May forecasts start with the atmospheric initial conditions of 9-13 April, 19-23 April and 29

April-3 May and ocean initial states specified from pentads centered at 11 April, 21 April and 1 May. The forecasts of other months of the year are selected in the same way. For verification of precipitation, the Climate Prediction Center Merged Analysis of Precipitation (CMAP; Xie and Arkin 1996), the R2 precipitation and the gridded daily rainfall data set from the India Meteorological Department (IMD; Rajeevan et al. 2006) are used. The circulation data from R2 reanalysis are used for verifying the horizontal wind fields.

b. DEMETER models

The DEMETER project uses seven coupled ocean-atmosphere models from the following European institutions: (1) European Centre for Research and Advanced Training in Scientific Computation (CERFACS), France, (2) European Centre for Medium-Range Weather Forecasts (ECMWF), (3) Istituto Nazionale de Geofisica e Vulcanologia (INGV), Italy, (4) Laboratorie d'Océanographie Dynamique et de Climatologie (LODYC), France, (5) Max-Planck Institut für Meteorologie (MPI), Germany, (6) Centre National de Recherches Météorologiques (Météo-France), France and (7) Met Office, United Kingdom. Hereafter, these models will be referred to as CERF, ECMW, INGV, LODY, MAXP, METF and UKMO, respectively. The main objective of the DEMETER project was to test the concept of multimodel ensemble prediction. The results of DEMETER have led to routine multi-model ensemble seasonal predictions at the ECMWF. In this study, however, the individual DEMETER models will be compared with each other.

The DEMETER produced 6-month long retrospective forecasts with each model from the initial conditions of 1 February, 1 May, 1 August and 1 November for the period 1980-2001. Each forecast set consists of an ensemble of nine members. Different initial conditions for the nine ensemble members are provided by three different ocean analyses and SST perturbations.

The atmospheric initial conditions are taken from the ECMWF 40-year reanalysis (ERA-40). The retrospective forecasts from 1 May initial conditions are used in this study in order to cover the monsoon season. Palmer et al. (2004) have provided the details of the DEMETER models and their retrospective forecasts. For verification purpose in the present study, the precipitation from the IMD data set and R2 reanalysis and SST from the Hadley Centre have been used.

3. Daily predictability

The daily mean monsoon rainfall and circulation simulated by the CFS forecasts is discussed in detail by Rai and Krishnamurthy (2011). The daily climatological mean rainfall and horizontal fields were found to simulate the seasonal cycle of onset, peak and withdrawal of monsoon fairly well. However, the magnitude and the spatial structure of the climatology in the CFS were not found to have good correspondence with the observations. The mean seasonal cycles of the DEMETER model is discussed by Joseph et al. (2010) who show that the multi-model ensemble mean is better compared to the individual models.

In this section, the predictability of the models in forecasting the daily means of rainfall and circulation is discussed in more detail. The predictability of the CFS analyzed by Rai Krishnamurthy (2011) and Krishnamurthy and Rai (2011) is reviewed, and new results on the predictability of the DEMTER models are presented. The errors in forecasts result from the imperfections of the model as well as due to the sensitive dependence on initial conditions in nonlinear systems. Therefore, the predictability of the model can be quantified by the following two measures. One of them is the forecast error defined as the difference between the prediction and observation. The other is the predictability error defined as the difference between two predictions made by the same model. The predictability errors arise solely due to the

uncertainties in the initial conditions under the assumption that the model is perfect while the forecast errors are caused by imperfections in both the initial conditions and the model (Lorenz 1982, 1985). The forecast errors and predictability errors give the lower and upper bounds of the predictability of a model, respectively (Lorenz 1982).

For a quantitative analysis of the monsoon predictability, it is useful to work with the following indices of rainfall and circulation over the monsoon region: (1) the Indian monsoon rainfall (IMR) index defined as the rainfall averaged over land points in India, (2) the extended Indian monsoon rainfall (EIMR) index defined as the rainfall averaged over (70°E-110°E, 10°N-30°N) (Goswami et al. 1999), (3) the Asian-Australian monsoon rainfall (AAMR) index defined as the rainfall averaged over (40°E-160°E, 40°S-40°N) (Krishnamurthy and Shukla 2001), (4) the monsoon Hadley (MH) index defined as the meridional wind shear between 850 hPa and 200 hPa averaged over (70°E-110°E, 10°N-30°N) (Goswami et al. 1999), and (5) the Westerly Shear (WS) index defined as the zonal wind shear between 850 hPa and 200 hPa averaged over (40°E-80°E, 5°N-20°N) (Wang and Fan 1999).

a. Forecast errors

The forecast errors (forecast minus observation) of daily IMR index in individual ensemble members for May and July initial conditions in CFS forecasts are shown as root mean square (RMS) errors in Fig. 1. The IMD rainfall data are used as observations. The root mean square (RMS) errors for each ensemble member are computed by averaging the squared forecast errors over the period 1981-2005. The initial size of the errors is in the ranges of 0.6–1.8 mm day^{-1} and 1.8–3.0 mm day^{-1} for the May and July forecasts, respectively. Although the time taken to reach saturation is different for the May and July forecasts, the errors in both cases reach

saturation by 1 July. These differences in the error growth are related to the fact that the May and July initial conditions occur during the onset and peak phases of the monsoon. For the EIMR index, which includes part of the oceanic region, Rai and Krishnamurthy (2011) have shown that the errors grow slightly faster for the May forecasts while the errors in the July forecasts are similar compared the error growth of the IMR index. Interestingly, the forecast errors of WS index (zonal circulation index) take about 20-30 days to reach saturation for May forecasts while it seems to take much longer to reach saturation for July forecasts, as shown by Krishnamurthy and Rai (2011).

The overall growth of forecast errors is studied by analyzing the RMS errors obtained by averaging the squared errors over all the ensemble members and over all the years (1981-2005). These RMS errors of the IMR and EIMR indices are shown in Fig. 2 for May and July forecasts. The errors in the IMR index shown in Fig.2 are with respect to both the IMD observation and R2 analysis whereas the errors in the EIMR index are with respect to R2 analysis only. The initial size of the errors is about 1 and 2 mm day^{-1} for the May and July forecasts, respectively. In the May forecasts, the IMR and EIMR indices take about 60 and 90 days, respectively, to reach saturation, thus indicating different growth rates (Figs. 2a, b). The errors with respect to IMD observations are higher by about 0.5–1.0 mm day^{-1} compared to the errors with respect to analysis (Fig. 2a). In July forecasts, the errors reach saturation in about 30 days for both the IMR and EIMR indices (Figs. 2c, d). The saturation value keeps decreasing steadily toward the end of the monsoon season.

The forecast errors of WS and MH circulation indices were also examined by Krishnamurthy and Rai (2011). Since the magnitudes of the zonal and meridional winds differ widely, the RMS forecast errors of WS and MH indices are shown along with the RMS errors of

zonal and meridional winds at 850 hPa and 200 hPa separately in Fig. 3 for May and July initial conditions. In May forecasts, the errors in the lower level winds grow at a slower rate and reach saturation in about 40 days (Figs. 3a, b). However, the errors in the upper level winds and the errors in the WS and MH indices grow at a much faster rate at first reaching saturation in about 20 days. Subsequently, the errors decay for a while up to day 130 and then grow again but at a slower rate. The two growing phases happen to occur during the onset and withdrawal phases of the monsoon. The errors in the July forecasts also reveal similar behavior but with some differences (Figs. 3c, d). The WS index, MH index and the horizontal winds at 200 hPa grow at a faster rate and reach saturation in about 20 days. This saturation level lasts for a shorter period of time (compared to May forecasts) and then the errors grow at a slower rate starting from day 60 when the withdrawal phase of the monsoon has started but before the monsoon ends.

The RMS forecast errors of the IMR index in all the DEMETER models are shown in Fig. 4. The forecast errors are with respect to IMD observed rainfall, and the squared errors are averaged over all nine ensemble members and over the period 1980-2001 to obtain the RMS errors for each model. It should be recalled that all the DEMETER forecasts analyzed here start from 1 May. In general, the error growths in the DEMETER models (Fig. 4) are similar to the error growth of the May forecast of the CFS (Fig. 1a). While some models (CERF, MAXP, METF and UKMO) reach saturation in about 60 days (by 1 July), other models (ECMW, INGV and LODY) reach saturation by 1 June. MAXP has the lowest saturation value. All models, except UKMO, show an initial slow growth during the monsoon onset period followed by a faster growth rate.

b. Predictability errors

Under the assumption that the model is perfect, the predictability error is the difference between two forecasts of the same model starting with different initial conditions. The predictability errors in the CFS model were analyzed by Rai and Krishnamurthy (2011) following a method used by Lorenz (1982) to determine the predictability of the ECMWF model. The Lorenz method is based on the idea that the one-day forecast of a particular day can be considered to be that day's analysis plus a moderately small error. Thus, the subsequent difference between two forecasts initiated one day apart gives the evolution of a presumably small initial error and will be referred to as 1-day predictability error. Similarly, forecasts starting from initial conditions that are two days apart provide 2-day predictability error, and so on.

There are 12 such pairs of forecasts that start one day apart in each month's CFS forecasts. The RMS predictability errors are then computed by averaging the squared errors over all the 12 pairs and over all the years (1981-2005). The RMS 1-day predictability errors of IMR and EIMR indices in the CFS are shown in Fig. 5 for May and July forecasts. The general pattern of the growth of predictability errors (Fig. 5) is similar to that of the forecast errors (Fig. 2). The predictability errors of the EIMR index have a higher saturation value, presumably due to the higher variability of the model forecasts over the Bay of Bengal and the Arabian Sea. The initial size of the predictability errors is large in the July forecasts since they start during the peak of the monsoon season. The growths of 1-day to 4-day predictability errors of IMR, EIMR and AAMR are discussed in more details by Rai and Krishnamurthy (2011).

The predictability errors of the circulation indices in the CFS were also examined by Krishnamurthy and Rai (2011). The evolution of 1-day predictability errors of WS and MH indices are shown in Fig. 6 along with those of the zonal and meridional winds at 850 hPa and 200 hPa for May and July CFS forecasts. In this case also, the predictability errors (Fig. 6) are

similar to the forecast errors (Fig. 3). A noticeable difference is in the May forecasts which show less decay after the first saturation (Figs. 6a, b). Also, the slower growths of the upper level zonal wind and the WS index (Fig. 6c) start earlier than in the case of the forecast errors (Fig. 3c).

Since all the integrations of the DEMETER models start on the same day (1 May) but with perturbed initial conditions, it is not necessary to follow the Lorenz method to compute the predictability errors in this case. Assuming each ensemble member to be perfect (or assumed to be observation), one at a time, the other members are treated as forecasts. In this way, for each DEMETER model, there are 36 "observation"-forecast pairs for each year. The RMS predictability error of the IMR index is computed from the averages of squared errors over all 36 members and over all the years and is shown for all the DEMETER models in Fig. 7. In general, the growth of the predictability errors (Fig. 7) is similar to that of the forecast errors (Fig. 4). However, the saturation values of the predictability errors are generally smaller than those of the forecast errors. In the case of MAXP, there is no clear error growth which implies that the forecasts of all the ensemble members are close to each other. An examination of the individual forecasts has shown that the daily anomalies of rainfall drift rapidly toward very small values in the IMR and EIMR regions in all the ensemble members. The MAXP model is known to have a large climate drift (Jin et al. 2008). In all the other models, the initial growth of predictability errors is smoother and does not reveal two different growth rates as in the case of forecast errors.

The saturation values reached by the forecast errors and predictability errors depend on the time mean and variance of the observations/analyses and forecasts, respectively. The saturation value of forecast errors (predictability errors) is simply the RMS difference between randomly selected observations (forecasts) and is about $\sqrt{2}$ times the standard deviation of the observations (forecasts). If the observations/analyses and forecasts have same mean and

variance, the forecasts errors and predictability errors will reach the same saturation value. In the case of DEMETER models, the saturation values of the forecast errors (Fig. 4) are slightly higher than those of the predictability errors (Fig. 7). This may imply that the model imperfections have contributed to the increased saturation value in the forecast errors. The seasonal character of the monsoon is reflected in the decreasing saturation level as the monsoon season progresses. In the case of CFS, the forecast errors of the IMR index using the IMD observation (Figs. 2a,c) seem to saturate at slightly higher values than the corresponding values of the predictability errors (Figs. 5a,c). However, the saturation values of the forecast errors using the analysis (Fig. 2) are actually less than those of the predictability errors (Fig. 5). The reasons for this behavior may be due to the fact that each ensemble member in the CFS forecasts spans different time periods during the monsoon season and that the analysis may have lower variance.

c. Estimate of error growth rate

In nonlinear dynamical systems, small initial errors first grow exponentially according to linear error dynamics and then slow down during the nonlinear phase of growth before reaching the saturation value (Lorenz 1985; Krishnamurthy 1993). The forecast errors and predictability errors of the models follow the same error growth pattern. To represent this typical error growth in large models, Lorenz (1982) introduced an empirical formula which has been found to be useful in estimating the growth rate of small errors. If the magnitude of the error is E, then the Lorenz error equation is represented by

$$\frac{dE}{dt} = \lambda E - sE^2, \qquad (1)$$

where λ is the growth rate of the error and s satisfies the condition that $E_s = \lambda/s$ is the saturation value of E. λ usually represents the first Lyapunov exponent of the system (Krishnamurthy 1993). If E_0 is the magnitude of the error at an initial time t_0, the solution to Eq. 1 is given by

$$E = \frac{1}{2} E_s \left[1 + \tanh\left[\frac{1}{2} \lambda (t - t_0) - \tanh^{-1}\left(1 - 2\frac{E_0}{E_s} \right) \right] \right]. \qquad (2)$$

The doubling time of small error is given by $t_d = (\ln 2)/\lambda$. The error growth rate can be estimated by fitting the error data to Eq. 2 using a suitable nonlinear least-squares method.

To demonstrate that Lorenz's empirical formula (Eq. 2) is a good approximation, the 1-day predictability error of the EIMR index in CFS May forecasts (from Fig. 5b) and its best fit of Eq. 2 are plotted in Fig. 8. Using Eq. 2, the nonlinear best fit curve has been extrapolated backward in time so that the initial linear growth is also included and the predictability error has been shifted forward in time in Fig. 8. The linear part of Eq. 1 is also plotted in Fig. 8 showing the exponential growth. The estimated value of λ is 0.08 which translates to a doubling time of 8.6 days for small errors. Although Eq. 2 is a good approximation, the initial value of the predictability error is found to be large enough to fall in the nonlinear regime of error growth.

All the predictability errors that were discussed earlier were fitted with the Lorenz's empirical formula to estimate the growth rate of small errors. For the predictability errors in the CFS (Fig. 5), the doubling times of the IMR and EIMR index are found to be 13.9 and 8.6 days, respectively, for the May forecasts while the corresponding values for the July forecasts are 4.1 and 6.9 days, respectively. These estimates clearly show the difference between the growth of initially small errors during the onset and peak phases of the monsoon. The error growth rates were also estimated for the predictability errors of the IMR index for all the DEMETER models (Fig. 7) except MAXP which does not show clear error growth. The doubling time of small

errors was found to be 4.6, 3.9, 6.9, 5.0, 4.6 and 4.1 days for CERF, ECMW, INGV, LODY, METF and UKMO, respectively. These values are comparable to the July CFS forecasts. Krishnamurthy and Rai (2011) have shown that two separate empirical formulas with fast and slow growth rates have to be fitted for the predictability errors in the circulation indices of CFS forecasts (Fig. 6). For example, the doubling time for fast and slow growth in the 200 hPa WS domain zonal wind of May forecasts (Fig. 6a) is found to be 4 and 23 days, respectively.

d. Active and break phases

Some studies (e.g., Waliser et al. 2003, Fu et al. 2007) have reported that the break periods of the monsoon are better predictable than the active periods. Since the CFS forecasts start with initial conditions spread throughout the monsoon season, Rai and Krishnamurthy (2011) were able to investigate whether predictability depends on the phase of the active/break cycle. Using the IMR index of analysis (R2), the active, break and normal periods are identified by the same criteria used by Krishnamurthy and Shukla (2007) and Rai and Krishnamurthy (2011). The normal periods are further separated by whether the evolution is from normal to active (normal-A) or from normal to break (normal-B). The RMS errors of 1-day predictability errors starting from initial conditions in these four intraseasonal phases are computed separately by using May, June, July and August forecasts.

The RMS predictability errors of IMR and EIMR indices of CFS forecasts initiated during the four phases of the active/break cycle are shown in Fig. 9. In the case of the IMR index, the errors starting from active and break phases show similar growth at a faster rate before reaching the saturation level in about 20-30 days (Fig. 9a). The doubling time of small errors for these two phases was estimated to be 2.0 days by fitting Lorenz's formula (Eq. 2). The errors

starting from both normal-A and normal-B phases grow slowly with an estimated doubling of small errors to be 8.6 days and reach saturation in about 50-60 days (Fig. 9a). The predictability errors of the EIMR index starting from all the four phases of the active/break cycle show similar growth behavior. In the case of WS circulation index also, there is no distinction in the error growth patterns from the four phases (Krishnamurthy and Rai 2011). Thus, the CFS does not show any preference in the predictability of either the active phase or the break phase. However, the CFS shows that the forecasts with initial conditions in both the active and break phases have lower predictability than the forecasts initiated during the transition from normal to active and normal to break phases.

4. Seasonal predictability

Because of the highly seasonal nature of the monsoon and the dependence of various socio-economic sectors on the entire season's rainfall, prediction of seasonal mean monsoon is very important. In this section, the predictability of the CFS in forecasting the seasonal mean monsoon discussed by Drbohlav and Krishnamurthy (2010) is reviewed and new results of the seasonal predictability of the DEMETER models are presented. Some aspects of the climatological mean monsoon rainfall and circulation in the CFS forecasts are also described by Drbohlav and Krishnamurthy (2010) and Yang et al. (2008). The June-September (JJAS) climatological means of CFS forecasts show excess rainfall in the Arabian Sea and deficient rainfall in the Bay of Bengal and over India. Although the climatological mean low-level winds are similar to those in the analysis, the forecasts underestimate the magnitude. The analysis of the climatological mean seasonal rainfall in the DEMETER models by Joseph et al. (2010) shows that only INGV and UKMO models realistically capture the spatial pattern over India.

a. Interannual variability

The JJAS seasonal anomalies of rainfall and circulation indices in the CFS forecasts are compared with observations/analysis in Fig. 10. The indices of the ensemble means are plotted for forecast leads of one to five months along with observation/analysis (CMAP and R2). The seasonal anomaly of the surface temperature averaged over the Niño-3 region (150°W-90°W, 5°S-5°N) is also shown. The forecasts are less accurate for the indices representing India and its neighborhood (IMR, EIMR and MH; Figs. 10a-c) compared to those representing the Indian and Pacific oceans (AAMR and Niño-3; Figs. 10d-e). These relations are confirmed by the values of the correlation between forecasts and observations (Drbohlav and Krishnamurthy 2010). By examining the composites of strong and weak events based on these various indices, Drbohlav and Krishnamurthy (2010) concluded that the CFS captures more accurately the ENSO-related features of the monsoon than the regionally influenced features of the monsoon.

The DEMETER models also show a similar behavior in the interannual variability of the forecasts. In Fig. 11a, the JJAS seasonal anomalies of the EIMR index of ensemble means of the DEMETER models are plotted along with the observed seasonal anomaly (CMAP). Similar time series of the Niño-3 index of the SST is also shown in Fig. 11b. While most of the DEMETER models have been able to forecast the interannual variability of the ENSO variability in SST, no model has captured the observed interannual variability of the EIMR index. In fact, the correlations between the model forecasts and the observation for EIMR index are less than 0.35 whereas corresponding correlations for Niño-3 index are in range 0.7−0.8. Another noticeable feature of the Niño-3 index forecasts is that four models (CERF, INGV, LODY and METF) which use the same ocean model (but slightly different versions) are all grouped together (Fig.

11b). The relations seen in these predictions indicate that the coupled ocean-atmosphere interactions in the Pacific and Indian Oceans that affect the monsoon need improvement.

b. Forecast errors

The predictability of the coupled models in forecasting the seasonal mean monsoon rainfall is first assessed by examining the forecast errors. The difference in the JJAS seasonal anomaly of rainfall over the monsoon region between CFS forecast and observation (CMAP) is expressed as RMS error by averaging over all ensemble members and over all the years. These RMS forecast errors are plotted in Figs. 12a-c for forecast leads of 1, 3 and 5 months, respectively. In the 1-month lead forecast (Fig. 12a), large values (above 3 mm day^{-1}) of the forecast error are in the Bay of Bengal, northeast India, the Arabian Sea along the west coast and the eastern equatorial Indian Ocean. These are the only regions where the magnitude of the error increases (slightly) from 1-month to 5-month lead. In 5-month lead forecast, the errors increase in a small region over the western equatorial Indian Ocean. Over most of the land points in India, the errors are in the range of 0.8–2.4 mm day^{-1} and remain unchanged for all leads. A detailed description of the errors in the forecasts of each month of the monsoon season is provided by Drbohlav and Krishnamurthy (2010).

The RMS forecast errors of JJAS seasonal anomalies of rainfall in DEMETER models are shown in Fig. 13. The spatial structure of the errors is generally the same for all the models but the magnitude varies. The common regions of large errors are in northeast India, Bay of Bengal and the equatorial Indian Ocean. Some of these features are similar to the forecast errors in CFS (Fig. 12a). The errors are smaller with remarkably similar spatial structure in CERF and

METF, perhaps because the two models have the same atmospheric component (ARPEGE) and same oceanic component although with different versions (OPA 8.2/8.0). However, other models (INGV and LODY) that use OPA oceanic component but different atmospheric components do not show the same error structure. It seems that the coupled models with same atmospheric component have similar error structure. Further examples of this behavior is seen in the errors of ECMW and LODY which have IFS as their atmospheric component and in the errors of INGV and MAXP which use ECHAM atmospheric model (different versions). The errors over the land points in India are larger in ECMW, LODY, and UKMO.

c. Predictability errors

The predictability errors of the seasonal mean forecasts under the assumption that the model is perfect are now examined. The predictability errors in the CFS are found by using the method of Lorenz (1982). Two forecasts initiated one month apart are considered and the difference between the JJAS seasonal anomalies of the two forecasts are averaged over all the ensemble members and all the years to obtain the RMS predictability error. The RMS errors, computed as a function of the lead forecast month, are shown in Figs. 12d-f for 1-, 3-, and 5-month lead, respectively. In this case also, large errors (above 3 mm day^{-1}) are in the Bay of Bengal, northeast India, the Arabian Sea along the west coast and the eastern equatorial Indian Ocean. The errors in these regions increase as the forecast lead increases. A detailed description of the predictability errors in the forecasts of each month of the monsoon season is provided by Drbohlav and Krishnamurthy (2010).

For the DEMETER models, the predictability errors are determined by assuming each ensemble member to be perfect, one at a time, while the other members are treated as forecasts.

The RMS errors are computed by taking the average over the ensemble pairs and all years. The RMS predictability errors in the DEMETER models are shown in Fig. 14. These predictability errors resemble the forecast errors (Fig. 13) in their spatial structure in all the models. In this case also, the models with the same atmospheric component have errors with similar spatial structure and magnitude (CERF and METF; ECMW and LODY). The low values of predictability error over India in MAXP should be treated with caution because the rainfall anomalies of all the ensemble members drift toward small values. Large errors in the equatorial oceanic region are seen in both ECMW and LODY, both of which use the IFS as the atmospheric component. The MAXP model, which has shown quite a different behavior compared to all other models, has been integrated with atmospheric and oceanic initial conditions and perturbation that are different what other models have used.

5. Prospects for decadal predictability

Recent years have seen an effort to extend climate prediction from seasonal time scale to decadal and multidecadal time scales. Prediction on decadal time scales is relevant for making long-term decisions to adapt to climate change and natural low-frequency variability of climate. In addition to the external forcing mechanisms, such as the variations in the solar radiation, the interactions within and between climate systems such as the atmosphere and ocean are sources of interdecadal variability. The existence of climate variability on different decadal time scales shown by several ocean-atmosphere coupled models provides hope for predictability at decadal time scale (Latif 1998). There are two different facets of decadal predictability. One is assessing the prediction of the decadal phenomenon itself (e.g., Boer 2000, Troccoli and Palmer 2007) while the other is concerned with the decadal modulation of the seasonal or interannual

phenomenon (e.g., Kirtman and Schopf 1998). Although several studies have indicated the possible predictability of phenomena related to Atlantic and Pacific oceans, the decadal prediction is still in infant stages. Because of lack of studies on decadal predictability of the Indian monsoon, a review of the relation of monsoon with known decadal phenomena is presented in this section.

Several studies have provided evidence for decadal variability of the Indian monsoon rainfall and circulation (e.g., Krishnamurthy and Goswami 2000). The IMR index is shown to have a low-frequency variability which alternates between above-normal epochs and below-normal epochs at about three-decade interval. An ENSO-like decadal variability is also known exist in the Pacific Ocean (Zhang et al. 1997). The decadal variations of IMR index and Niño-3 index were shown to vary together most of the time by Krishnamurthy and Goswami (2000). They further suggested that the El Niño (La Niña) may have enhanced relation with droughts (floods) whereas La Niña (El Niño) may not have a significant relation with the monsoon during the warm (cold) phase of the decadal variability. A similar relation was also found by Krishnan and Sugi (2003). In the North Pacific Ocean, the dominant mode of variability is the Pacific Decadal Oscillation (PDO) which varies with a time scale of about 20-30 years. Several studies have established that the North Pacific variability can cause decadal modulation of the variability of the tropical Pacific Ocean or ENSO (e.g., Barnett et al. 1999). This relation implies that the ENSO-monsoon relation can also be modulated by PDO. The influence of PDO on the monsoon variability has not been thoroughly investigated.

Another low-frequency oceanic mode of variability that may influence the monsoon is the Atlantic Multidecadal Oscillation (AMO) which occurs in the North Atlantic with a time scale of about 50-70 years. From model experiments and observations, Zhang and Delworth

(2006) indicated that warm (cold) phase of the AMO enhances (reduces) the Indian monsoon rainfall. They suggested that the warm AMO phase leads to a northward shift in the Intertropical Convergence Zone (ITCZ) which in turn is associated with anomalous southwesterly surface winds. Different mechanisms for the relation between AMO and the monsoon rainfall have been suggested by other studies (e.g., Goswami et al. 2006).

Since the time scales and phases of the AMO, PDO and the ENSO decadal oscillations vary, it is necessary to determine the combined influence of these decadal oscillations on the Indian monsoon. The prospect for decadal prediction of the Indian monsoon depends on the discernable influences of the decadal oscillations of the oceans and any other slowly varying component of the climate system on the monsoon. So far, not many model experiments have been performed with coupled ocean-atmosphere models to isolate the influences of the decadal variability of the Pacific and Atlantic oceans on monsoon.

6. Summary

The predictability of eight coupled ocean-atmosphere models in predicting the Indian monsoon rainfall and circulation has been reviewed. The retrospective forecasts of CFS, the operational coupled model of the NCEP, for the period 1981-2005 were analyzed. The retrospective forecasts of seven coupled models from the DEMETER, a project to test the concept of multimodel ensemble prediction, were analyzed for the period 1980-2001. The predictability of these eight models was studied at daily and seasonal time scales. The predictability is expressed in terms of forecast errors which include the imperfections in both the model and initial condition and predictability errors which depend solely on the uncertainties in the initial condition assuming the model to be perfect. The Lorenz method of analysis and the

Lorenz empirical formula were used to estimate the error growth rates. The relation between the Indian monsoon and the decadal oscillations of different ocean basins were also discussed.

The forecast errors and predictability errors in the daily forecasts of all the models follow the classic error growth pattern of nonlinear systems. The daily rainfall in the CFS showed differences in the initial size and error growth rate between forecasts with initial conditions in May and July, reflecting the different phases (onset and peak) of the monsoon season. The doubling time of small errors was estimated to be in the rage of 4-14 days for the IMR index and 7-9 days for the EIMR index, depending on the initial month of the forecast. The doubling time of small errors of the IMR index in the DEMETER models, all of which start with 1 May initial conditions, were estimated to be in the range of 4-7 days. The predictability of the horizontal winds in the CFS was found to be somewhat different from that of the rainfall. The error growth in the horizontal winds seems to be governed by two time scales, more pronounced in the upper level than in the lower level. The analysis of the dependence of predictability on the phase of the active/break cycle did not provide a clear picture. Only in the case of IMR index, there was a difference in the error growth rate between the forecasts initiated in normal phases and those initiated in peak active/break phases.

All the models (CFS and DEMETER) failed to capture the observed interannual variability of the JJAS seasonal anomalies of the rainfall index over the Indian monsoon region, especially during years of developing El Niño and La Niña events. However, all the models were able to predict the seasonal anomalies of the Niño-3 index with very high interannual correlation with observation. These coupled models are successful in simulating the ocean-atmosphere interaction in the Pacific Ocean region but not over the Indian monsoon region. The models still require improvement in capturing the seasonally persistent influences of the slowly varying

components of the coupled system according to Charney-Shukla hypothesis. The spatial structures of forecast errors and predictability errors were found be generally same in all the models. The errors are large in the Bay of Bengal, the Arabian Sea along the west coast of the Indian peninsula and the equatorial Indian Ocean. The analysis of the DEMETER models showed that the models which had the same atmospheric component produced errors with similar structure and magnitude.

The prospect for predicting the Indian monsoon on decadal time scales was addressed by reviewing the known relation between the monsoon and the decadal variability of different oceans. The ENSO-like decadal variability of the tropical Pacific Ocean seems to vary together with the Indian monsoon rainfall and may influence the severity of the droughts and floods. The PDO which influences the ENSO may also affect the variability of the monsoon through ENSO-monsoon relation. The Atlantic Ocean may also affect the monsoon on decadal time scale with the warm (cold) phase of the AMO enhancing (reducing) the Indian monsoon rainfall.

The dynamical seasonal prediction of the Indian monsoon rainfall remains a challenge. Both the AGCMs and the coupled models show large systematic errors in simulating the mean monsoon circulation and rainfall, the statistics of active and break cycles, and the number, intensity and tracks of monsoon lows and depressions. The models are unable to produce realistic simulation of the interannual variability of the monsoon. Even the AGCMs with observed but prescribed SST are unable to simulate the mean monsoon and its interannual variability. This has raised questions about the usefulness of AGCMs with prescribed SST in simulating and predicting the Indian monsoon circulation and rainfall.

Some recent forecast experiments by David Dewitt (personal communication) suggest that the dynamical predictions of seasonal mean monsoon circulation and rainfall from coupled

models are indistinguishable from seasonal forecasts if the same SSTs were prescribed (Tier 2). Similar conclusion has been reached by Edwin Schneider (personal communication) is a separate study. These model results, combined with the observational studies of Gadgil et al. (2004) and Krishnamurthy and Kirtman (2009) which showed robust relationships between SST anomalies over the Pacific and Indian oceans and the Indian summer monsoon rainfall, raise the following question which the present study cannot answer: Is the deficiency of AGCMs (with prescribed SST) in predicting the seasonal mean monsoon rainfall primarily due to lack of ocean-atmosphere coupled fluxes or lack of AGCMs ability to simulate the SST-forced response in heating and convergence?

Acknowledgments

This research was supported by grants from the National Science Foundation (ATM-0830068), National Oceanic and Atmospheric Administration (NA09OAR4310058), and National Aeronautics and Space Administration (NNX09AN50G).

References

Barnett, T. P., D. W. Pierce, M. Latif, D. Dommenget, and R. Saravanan, 1999: Interdecadal interactions between the tropics and midlatitudes in the Pacific basin. *Geophys. Res. Lett*. **26**, 615-618.

Boer, G. J., 2000: A study of atmosphere-ocean predictability on long time scales. *Clim. Dyn*., **16**, 469-472.

Charney, J. G., and J. Shukla, 1981: Predictability of monsoons. *Monsoon Dynamics*, J. Lighthill and R. P. Pearce, Eds., Cambridge University Press, 99-109.

DelSole, T., and J. Shukla, 2002: Linear prediction of Indian monsoon rainfall. *J. Climate*, **15**, 3645-3658.

Drbohlav, H.-K. L., and V. Krishnamurthy, 2010: Spatial structure, forecast errors, and predictability of the South Asian monsoon in CFS monthly retrospective forecasts. *J. Climate*, **23**, 4750-4769.

Fu, X., B. Wang, D. E. Waliser, and L. Tao, 2007: Impact of atmosphere-ocean coupling on the predictability of monsoon intraseasonal oscillations. *J. Atmos. Sci.*, **64**, 157-174.

Gadgil, S., M. Rajeevan, and R. Nanjundiah, 2005: Monsoon prediction – Why yet another failure? *Curr. Sci.*, **88**, 1389-1400.

Gadgil, S., P. N. Vinayachandran, P. A. Francis, S. Gadgil, 2004: Extremes of the Indian summer monsoon rainfall, ENSO and equatorial Indian Ocean oscillation. *Geophys. Res. Lett.*, **31**, doi:10.1029/2004GL019733.

Goswami, B. N., Krishnamurthy, V. and Annamalai, H., 1999: A broad-scale circulation index for the interannual variability of the Indian summer monsoon. *Quart. J. Roy. Meteor. Soc.*, **125,** 611–633.

Goswami, B. N., M. S. Madhusoodanan, C. P. Neema, and D. Sengupta, 2006: A physical mechanism for North Atlantic SST influence on the Indian summer monsoon. *Geophys. Res. Lett.,* **33**, L02706, doi:10.1029/2005GL024803.

Jin, E. K., and Co-authors, 2008: Current status of ENSO prediction skill in coupled ocean-atmosphere models. *Clim. Dyn.*, **31**, 647-664.

Joseph, S., A. K. Sahai, and B. N. Goswami, 2010: Boreal summer intraseasonal oscillations and seasonal Indian monsoon prediction in DEMETER coupled models. *Clim. Dyn.*, **35**, 651-667.

Kanamitsu, M., W. Ebisuzaki, J. Woollen, S.-K. Yang, J. J. Hnilo, M. Fiorino, and G. L. Potter, 2002: NCEP-DOE AMIP-II Reanalysis (R-2). *Bull. Amer. Meteor. Soc*., **83**, 1631-1643.

Kang, I.-S., and J. Shukla, 2006: Dynamical seasonal prediction and predictability of the monsoon. *The Asian monsoon*, B. Wang, Ed., Springer-Praxis, 585-612.

Kang, I.-S., K. Jin, B. Wang, K.-M. Lau, J. Shukla, V. Krishnamurthy, S. D. Schubert, D. E. Waliser, W. F. Stern, A. Kitoh, G. A. Meehl, M. Kanamitsu, V. Y. Galin, V. Satyan, C.-K. Park, Y. Liu, 2002: Intercomparison of the climatological variations of Asian summer monsoon precipitation simulated by 10 GCMs. *Climate Dyn.*, **19**, 383-395.

Kirtman, B. P., and P. S. Schopf, 1998: Decadal variability in ENSO predictability and

prediction. *J. Climate*, **11**, 2804-2822.

Krishnamurthy, V., 1993: A predictability study of Lorenz's 28-variable model as a dynamical system. *J. Atmos. Sci.*, **50,** 2215-2229.

Krishnamurthy, V., and B. N. Goswami, 2000: Indian monsoon-ENSO relationship on interdecadal timescale. *J. Climate*, **13,** 579-595.

Krishnamurthy, V., and J. L. Kinter III, 2003: The Indian monsoon and its relation to global climate variability. *Global Climate*, X. Rodó and F. A. Comín, Eds., Springer-Verlag, Berlin, 186–236.

Krishnamurthy, V., and B. P. Kirtman, 2009: Relation between Indian monsoon variability and SST. *J. Climate*, **22,** 4437–4458.

Krishnamurthy, V., and J. Shukla, 2000: Intraseasonal and interannual variability of rainfall over India. *J. Climate*, **13,** 4366-4377.

Krishnamurthy, V., and J. Shukla, 2001: Observed and model simulated interannual variability of the Indian monsoon. *Mausam*, **52,** 133-150.

Krishnamurthy, V., and J. Shukla, 2007: Intraseasonal and seasonally persisting patterns of Indian monsoon rainfall. *J. Climate*, **20,** 3-20.

Krishnamurthy, V., and J. Shukla, 2008: Seasonal persistence and propagation of intraseasonal patterns over the Indian monsoon region. *Clim. Dyn.,* **30**, 353-369.

Krishnamurthy, V., and S. Rai, 2011: Predictability of South Asian monsoon circulation in the NCEP Climate Forecast System. *Adv. Geosci.*, **22**, 65-76.

Krishnan, R., and M. Sugi, 2003: Pacific decadal oscillation and variability of the Indian summer monsoon rainfall. *Clim. Dyn.*, **21**, 233-242.

Kumar, K. K., M. Hoerling, and B. Rajagopalan, 2005: Advancing dynamical prediction of

Indian monsoon rainfall. *Geophys. Res. Lett.*, **32,** L08704, doi:10.1029/2004GL021979.

Latif, M., 1998: Dynamics of interdecadal variability in coupled ocean-atmosphere models. *J. Climate*, **11**, 602-624.

Lorenz, E. N., 1962: The statistical prediction of solutions of dynamic equations. *Proc. Int. Symp. Numerical Weather Prediction*, Tokyo, Japan, 629-635.

Lorenz, E. N., 1982: Atmospheric predictability experiments with a large numerical model. *Tellus*, **34,** 505-513.

Lorenz, E. N., 1984: Some aspects of atmospheric predictability. *Problems and prospects in long and medium range weather forecasting*, D. M. Burridge and E. Kallen, Eds., Springer-Verlag, Berlin, 1-20.

Lorenz, E. N., 1985: The growth of errors in prediction. *Turbulence and predictability in geophysical fluid dynamics and climate dynamics*, M. Ghil, R. Benzi, and G. Parisi, Eds., North Holland, Amsterdam, 243-265.

Moorthi, S., H. –L. Pan, and P. Caplan, 2001: Changes to the 2001 NCEP operational MRF/AVN global analysis/forecast system. NWS Tech. Procedures Bulletin 484, 14pp. [Available online at http://www.nws.noaa.gov/om/tpb/484.htm.]

Pacanowski, R. C., and S. M. Griffies, 1998: MOM 3.0 manual. NOAA/GFDL. [Available online at http://www.gfdl.noaa.gov/~smg/MOM/web/guide_parent/guide_parent.html.]

Palmer, T. N., and coauthors, 2004: Development of a European multimodel ensemble system for seasonal-to-interannual prediction (DEMETER). *Bull. Amer. Meteor. Soc.*, **85,** 853-872.

Palmer, T. N., C. Brankovic, P. Viterbo, and M. J. Miller, 1992: Modeling interannual variations of summer monsoons. *J. Climate*, **5,** 399-417.

Rai, S., and V. Krishnamurthy, 2011: Error growth in Climate Forecast System daily retrospective forecasts in South Asian monsoon. J. *Geophys. Res.*, **116**, D03108, doi:10.1029/2010JD014840.

Rajeevan, M., 2001: Prediction of Indian summer monsoon: Status, problems and prospects. *Curr. Sci.*, **81,** 1451-1457.

Rajeevan, M., J. Bhate, J. D. Kale, and B. Lal, 2006: High resolution daily gridded rainfall data for the Indian region: Analysis of break and active monsoon spells. *Current Science***, 91**, 296-306.

Rasmusson, E. M., and T. H. Carpenter, 1983: The relationship between eastern equatorial Pacific sea surface temperatures and rainfall over India and Sri Lanka. *Mon. Wea. Rev.*, **111,** 517-528.

Saha, S., S. Nadiga, C. Thiaw, J. Wang, W. Wang, Q. Zhang, H. M. Van den Dool, H.-L. Pan, S. Moorthi, D. Behringer, D. Stokes, M. Pena, S. Lord, G. White, W. Ebisuzaki, P. Peng, and P. Xie, 2006: The NCEP Climate Forecast System. *J. Climate*, **19,** 3483-3515.

Shukla, J., 1998: Predictability in the midst of chaos: A scientific basis for climate forecasting. *Science*, **282,** 728-731.

Sikka, D. R., 1980: Some aspects of the large scale fluctuations of summer monsoon rainfall over India in relation to fluctuations in the planetary and regional scale circulation parameters. *Proc. Indian Acad. Sci. (Earth & Planet. Sci.)*, **89,** 179-195.

Simmons, A. J., and A. Hollingsworth, 2002: Some aspects of the improvement in skill of numerical weather prediction. *Quart. J. Roy. Meteor. Soc*., **128**, 647-677.

Sperber, K. R., C. Brankovic, M. Déqué, C. S. Frederiksen, R. Graham, A. Kitoh, C. Kobayashi, T. Palmer, K. Puri, W. Tennant, and E. Volodin, 2001: Dynamical seasonal prediction of

the Asian summer monsoon. *J. Climate*, **129,** 2226-2248.

Sperber, K. R., and T. N. Palmer, 1996: Interannual tropical rainfall variability in general circulation model simulations associated with the Atmospheric Model Intercomparison Project. *J. Climate*, **9**, 2727-2750.

Troccoli, A., and T. N. Palmer, 2007: Ensemble decadal predictions from analysed initial conditions. *Phil. Trans. Roy. Soc. A,* **365**, 2179-2191.

Waliser, D. E., W. Stern, S. Schubert, and K. M. Lau, 2003: Dynamic predictability of intraseasonal variability associated with the Asian summer monsoon. *Quart. J. Roy. Meteor. Soc.*, **129**, 2897-2925.

Walker, G. T., 1923: Correlation in seasonal variations of weather. VIII. A preliminary study of world weather. *Indian Meteor. Memo.*, **24** (Part 4), 75-131. [Also published in *Sir Gilbert T. Walker - Selected Papers*, Indian Meteorological Society, New Delhi, 1986, 120-178.]

Walker, G. T., 1924: Correlation in seasonal variations of weather. IX. A further study of world weather. *Indian Meteor. Memo.*, **24** (Part 9), 275-332. [Also published in *Sir Gilbert T. Walker - Selected Papers*, Indian Meteorological Society, New Delhi, 1986, 179-240.]

Wang, B., Q. Ding, X. Fu, I.-S. Kang, K. Jin, J. Shukla, and F. Doblas-Reyes, 2005a: Fundamental challenge in simulation and prediction of summer monsoon rainfall. *Geophys. Res. Lett.*, **32,** L15711, doi:10.1029/2005GL022734.

Wang, B., and Z. Fan, 1999: Choice of South Asian summer monsoon indices. *Bull. Amer. Meteor. Soc.*, **80**, 629-638.

Xie, P. and Arkin, P. A., 1996: Analyses of global monthly precipitation using gauge observations, satellite estimates and numerical model predictions. *J. Climate*, **9**, 840-858.

Yang, S., Z. Zhang, V. E. Kousky, R. W. Higgins, S.-H. Yoo, J. Liang, and Y. Fan, 2008: Simulations and seasonal prediction of the Asian summer monsoon in the NCEP Climate Forecast System. *J. Climate*, **21,** 3755-3775.

Zhang, R., and T. L. Delworth, 2006: Impact of Atlantic multidecadal oscillations on India/Sahel rainfall and Atlantic hurricanes. *Geophys. Res. Lett*., **33**, L17712, doi:10.1029/2006GL026267.

Zhang, Y., J. M. Wallace, and D. S. Battisti, 1997: ENSO-like interdecadal variability: 1900–93. *J. Climate,* **10**, 1004–1020.

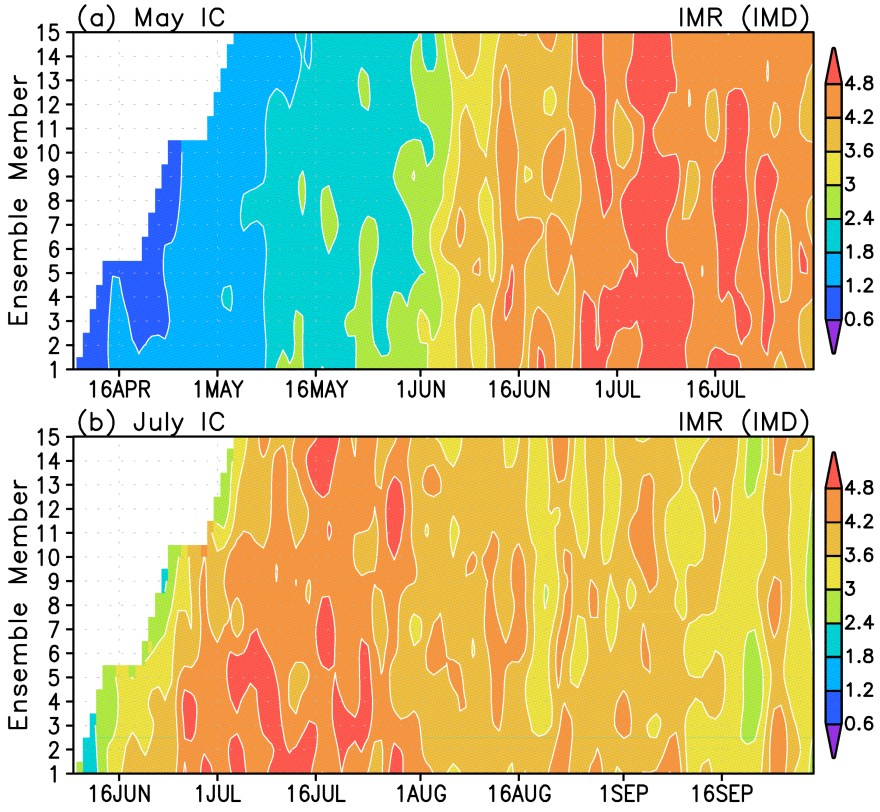

Fig. 1. CFS Forecast errors: RMS errors of IMR index of individual ensemble members starting from (a) May and (b) July initial conditions. The errors are differences between forecasts and IMD observed rainfall. The RMS errors are calculated by averaging the squared errors over the years 1981-2005. Units are in mm day^{-1}.

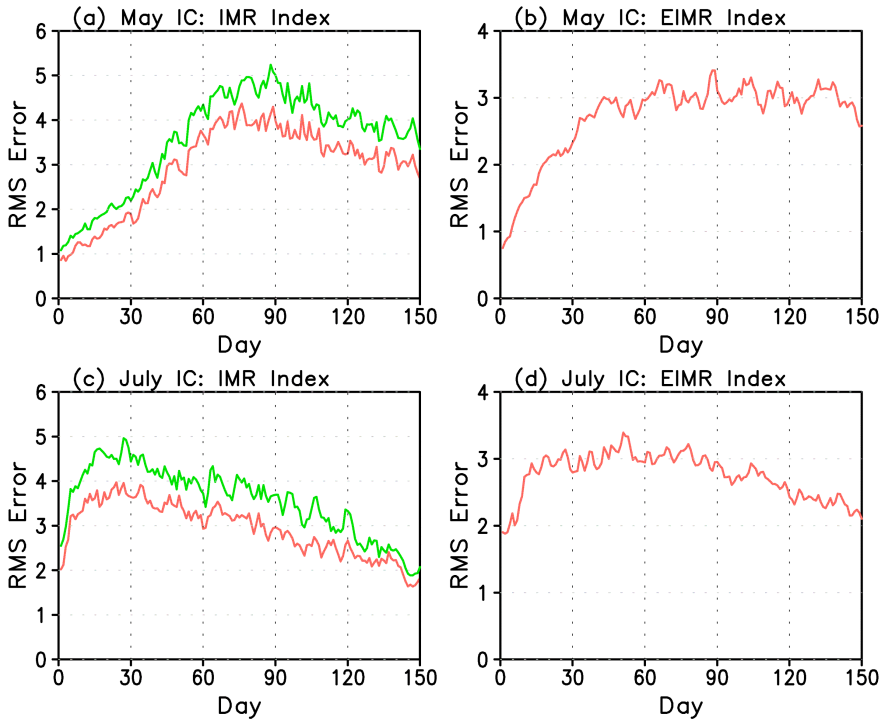

Fig. 2. Forecast errors in CFS: RMS errors of IMR index for (a) May and (c) July initial conditions and RMS errors of EIMR index for (b) May and (d) July initial conditions. The RMS errors are computed by averaging the squared errors over all ensemble members and over the years 1981-2005. Day zero refers to the first forecast day of each of the 15 individual ensemble members. Errors with respect to observed IMD rainfall are also shown (green) for comparison with errors with respect to analysis (red). Units are in mm day^{-1}.

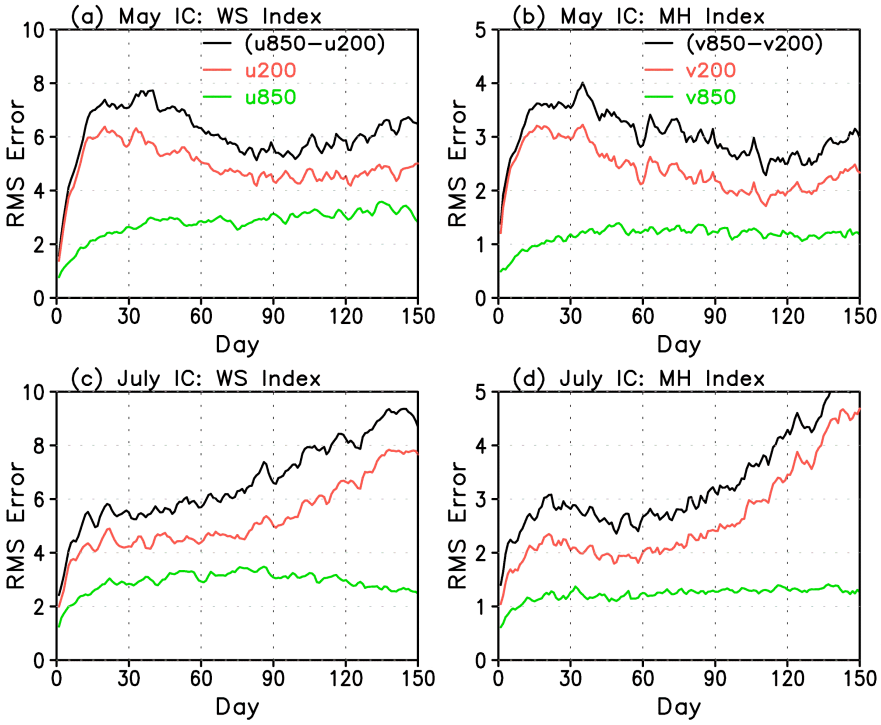

Fig. 3. Forecast errors in CFS: RMS errors of WS-domain-averaged $u850$ (green), $u200$ (red) and ($u850-u200$) (black) for (a) May and (c) July initial conditions. RMS errors of MH-domain-averaged $v850$ (green), $v200$ (red) and ($v850-v200$) (black) for (b) May and (d) July initial conditions. The RMS errors are computed by averaging the squared errors over all ensemble members and over the years 1981-2005. Day zero refers to the first forecast day of each of the 15 individual ensemble members. Units are in m s^{-1}.

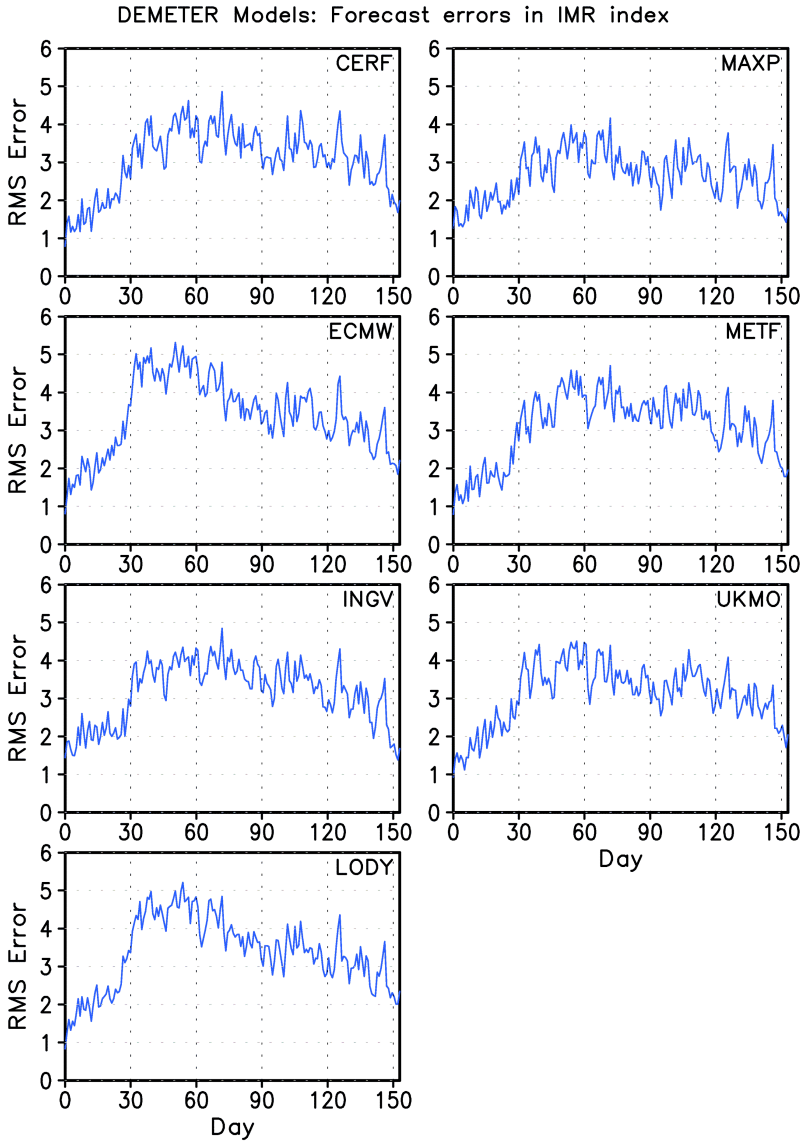
DEMETER Models: Forecast errors in IMR index
CERF
MAXP
ECMW
METF
INGV
UKMO
LODY
RMS Error
Day
0
1
2
3
4
5
6
0
30
60
90
120
150

Fig. 4. Forecast errors in DEMETER models: RMS errors of IMR index using IMD rainfall data as observation. The RMS errors are computed by averaging the squared errors over all ensemble members and over the years 1980-2001. Day zero refers to the first forecast day of each of the 9 individual ensemble members. The model is identified in the top right corner of each panel. Units are in mm day^{-1}.

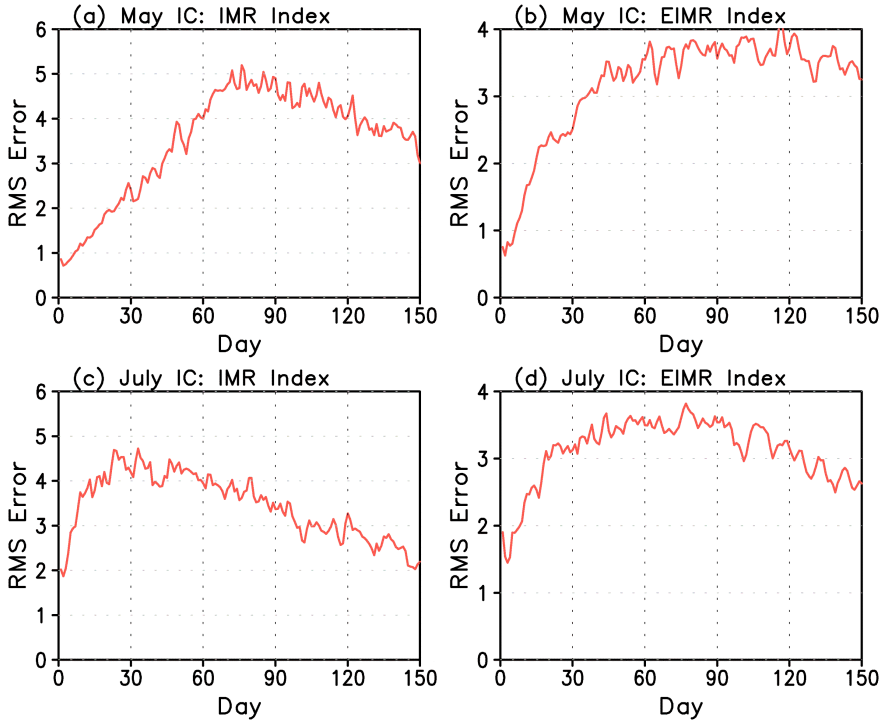

Fig. 5. Predictability errors in CFS: RMS 1-day predictability errors of IMR index for (a) May and (c) July initial conditions and forecast errors of EIMR index for (b) May and (d) July initial conditions. The RMS errors are computed by averaging the squared errors over all ensemble member pairs in the 1-day predictability errors and over the years 1981-2005 (see text for details). Units are in mm day^{-1}.

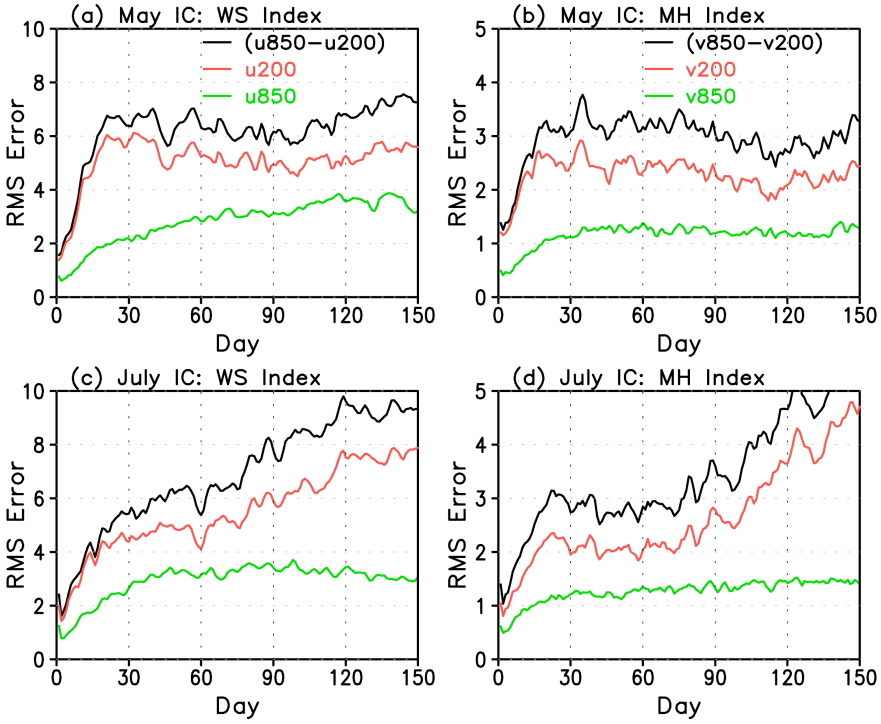

Fig. 6. Predictability errors in CFS: RMS 1-day predictability errors of WS-domain-averaged *u*850 (green), *u*200 (red) and (*u*850−*u*200) (black) for (a) May and (c) July initial conditions. RMS errors of MH-domain-averaged *v*850 (green), *v*200 (red) and (*v*850−*v*200) (black) for (b) May and (d) July initial conditions. The RMS errors are computed by averaging the squared errors over all ensemble member pairs in the 1-day predictability errors and over the years 1981-2005 (see text for details). Units are in m s^{-1}.

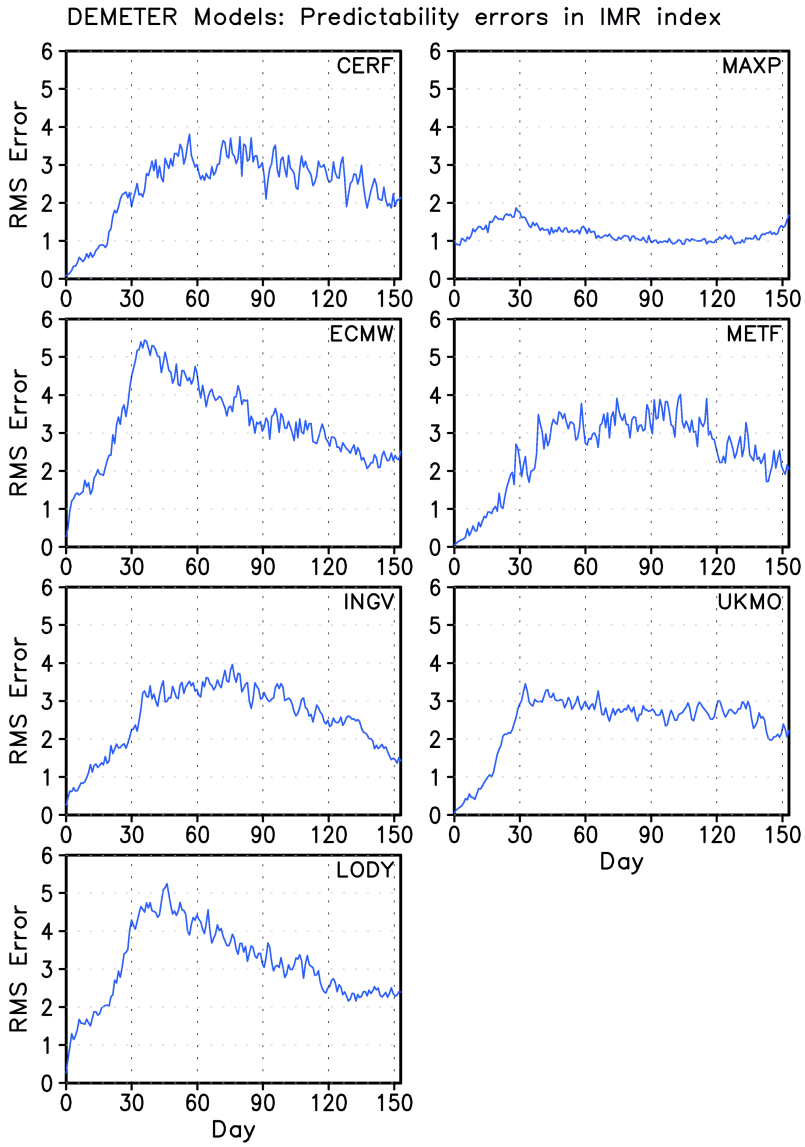

Fig. 7. Predictability errors in DEMETER models: RMS predictability errors of IMR index.

Units are in mm day^{-1}. The RMS errors are computed by averaging the squared errors over all ensemble member pairs in the predictability errors and over the years 1980-2001 (see text for details). The model is identified in the top right corner of each panel.

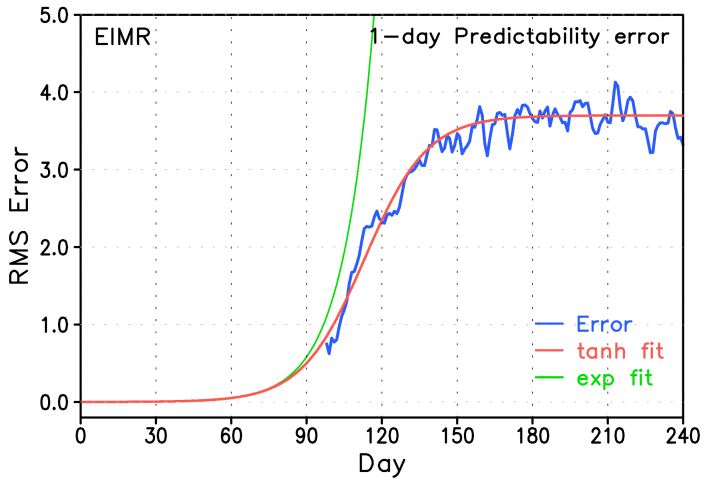

Fig. 8. RMS error (blue) of EIMR index, empirical fit (green) according to eq. 2 and empirical fit (red) according to eq. 4. The RMS error is 1-day predictability error in CFS (same as that in Fig. 5b) with May initial condition. The predictability error curve (blue) has been shifted forward in time so that the fitted curves (red and green) are extrapolated back to start with a very small initial error (~10^{-3}) at day zero.

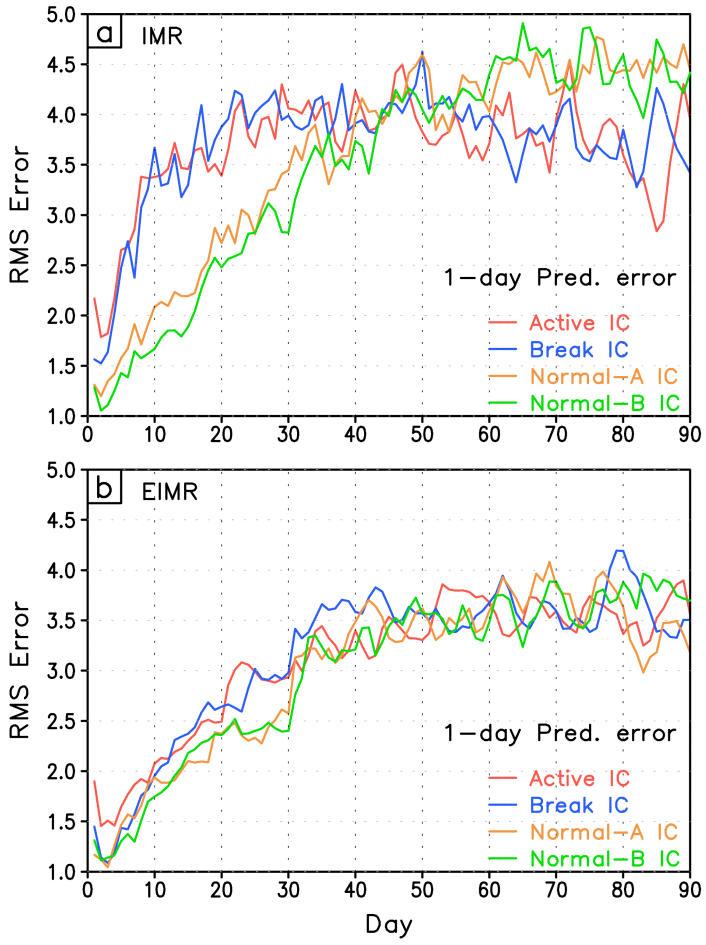

Fig. 9. CFS predictability errors: RMS 1-day predictability errors of (a) IMR index and (b) EIMR index shown separately for initial conditions starting from active (red), break (blue), normal-A (orange) and normal-B phases (green). May, June, July and August forecasts are used in computing the RMS errors. The RMS errors are computed by averaging the squared errors over all ensemble member pairs in the 1-day predictability errors and over the years 1981-2005 (see text for details). Units are in mm day^{-1}.

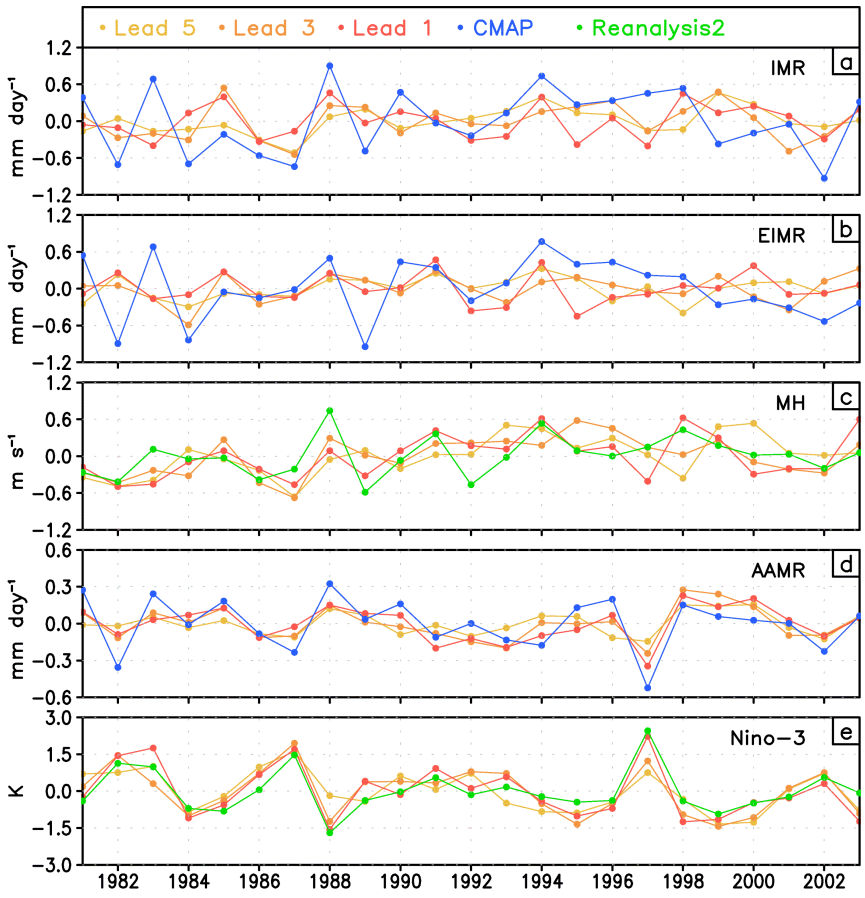

Fig.10. CFS forecasts: JJAS seasonal anomalies of (a) IMR, (b) EIMR, (c) MH, (d) AAMR, (e) WY, and (f) Niño-3 indices in observation (CMAP)/analysis and forecasts for 1-, 3- and 5-month leads.

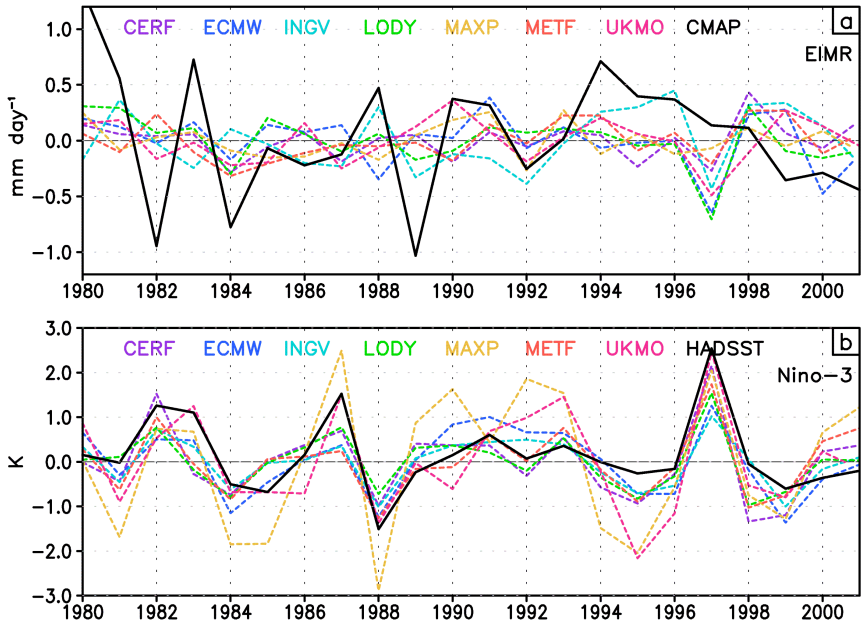

Fig.11. DEMETER model forecasts from 1 May initial conditions: JJAS seasonal anomalies of (a) EIMR and (b) Niño-3 indices in ensemble mean of model forecasts and observations (CMAP for precipitation and HadISST for SST).

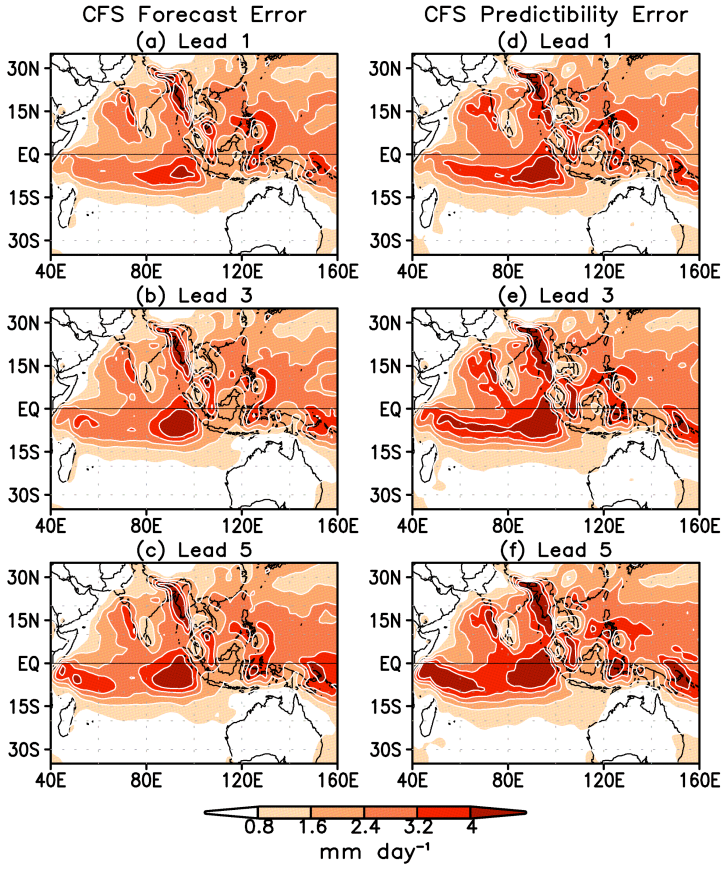

Fig.12. CFS forecasts: Forecast error of seasonal precipitation shown as RMSE of JJAS mean precipitation anomalies between forecast (1-, 3- and 5-month lead) and observation (left panels). Predictability error of the model for *n*-month lead shown as RMSE of JJAS seasonal precipitation anomalies between *n*-month lead forecast and (*n*-1)-month lead forecast (right panels). The RMS errors are calculated by averaging the squared errors over all ensemble members and over the years 1981-2005. Units are in mm day^{-1}.

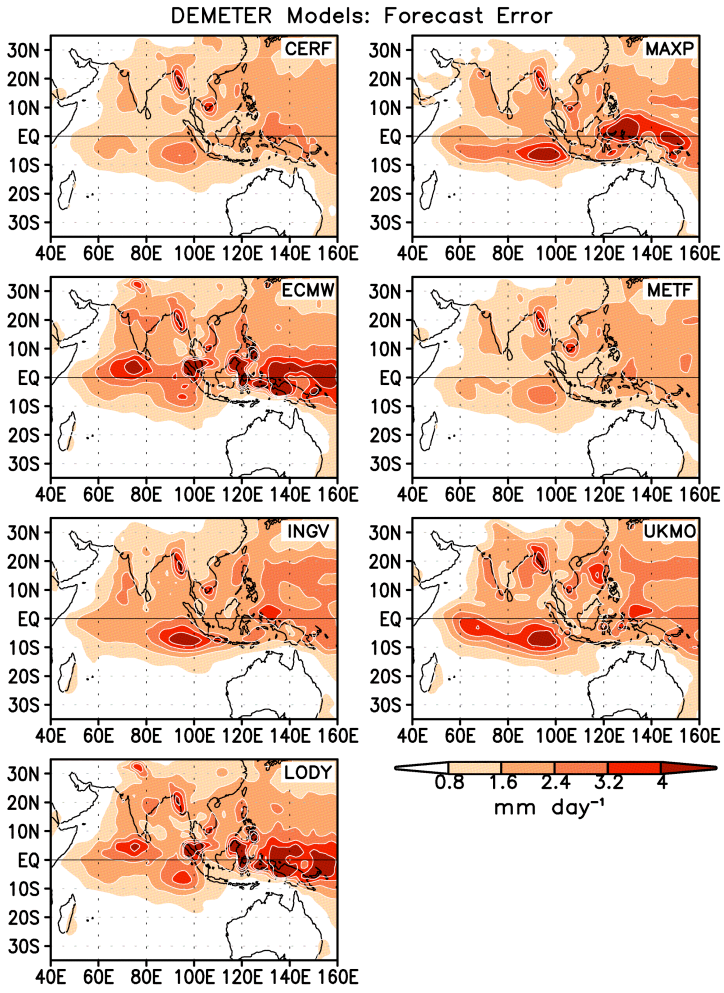

Fig.13. DEMETER model forecasts from 1 May initial conditions: RMS forecast errors of JJAS seasonal precipitation anomalies. Units are in mm day^{-1}. The RMS errors are calculated by averaging the squared errors over all ensemble members and over the years 1980-2001. The model is identified in the top right corner of each panel.

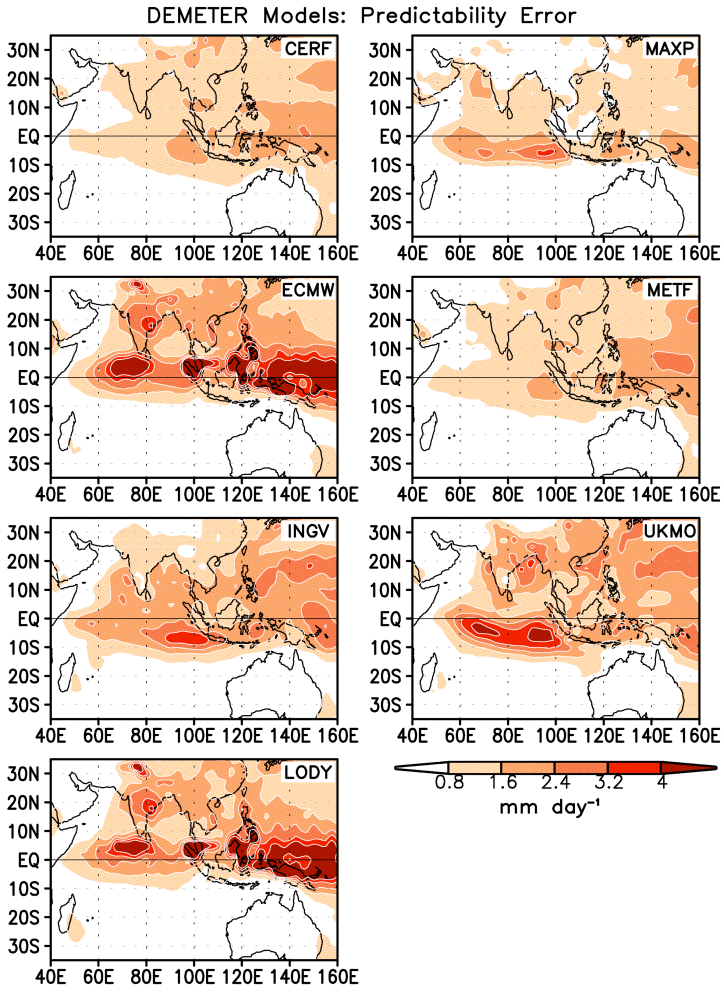

Fig.14. DEMETER model forecasts from 1 May initial conditions: RMS predictability errors of JJAS seasonal precipitation anomalies. Units are in mm day^{-1}. The RMS errors are calculated by averaging the squared errors over all ensemble members and over the years 1980-2001. The model is identified in the top right corner of each panel.